Studies on transparent spinel magnesium indium oxide thin films prepared by chemical spray pyrolysis

A. Moses Ezhil Raj [b], V. Senthilkumar [a], V. Swaminathan [c], Joachim Wollschläger [d], M. Suendorf [d], M. Neumann [d], M. Jayachandran [e], C. Sanjeeviraja [a,*]

[a] Department of Physics, Alagappa University, Karaikudi-630 003, India
[b] Departments of Physics, Scott Christian College (Autonomous), Nagercoil-629 003, India
[c] School of materials Science and Engineering, Singapore 639 798, Singapore
[d] Fachbereich Physik, Universität Osnabrück, D-49069, Germany
[e] ECMS Division, Central Electrochemical Research Institute, Karaikudi-630 006, India

ARTICLE INFO

ABSTRACT

Ternary semiconducting oxide compound magnesium indium oxide films ($MgIn_2O_4$), manifesting high transparency were prepared by metal organic chemical spray pyrolysis technique. Precursors prepared for various cationic ratios of Mg/In = 0.35, 0.40, 0.45 and 0.50 were thermally sprayed onto quartz substrates, decomposed at 450 °C and the spinel phase evolution was studied. X-ray diffraction, Rutherford backscattering and X-ray photoelectron spectroscopy studies have been conducted to confirm the formation of single-phase $MgIn_2O_4$ films with Mg/In ratio 0.50. From optical transmission studies, the observed optical band gaps varied from 3.18 to 3.86 eV ($0.35 < Mg/In < 0.5$). The electrical conductivity variations of these films were measured in the temperature range between 30 and 150 °C by four-probe technique ($34.07–1.44 \times 10^{-5}$ S cm^{-1}) and the Hall coefficient showed n-type electrical conduction and high carrier concentration ($0.16 \times 10^{20}–0.89 \times 10^{17}$ cm^{-3}).

© 2008 Elsevier B.V. All rights reserved.

1. Introduction

In recent years, considerable attention has been given to wide gap materials with optical transparency and metallic conductivity in the development of transparent electrodes in liquid crystal displays and solar cells. For transmission of visible light, the optical band gap must be greater than 3 eV. Despite their large band gaps, they can sustain a high concentration of electrons with high carrier mobility. Materials exhibiting these properties are almost limited to oxides, fluorides and chlorides. In the periodic table, the fifth row elements are n-type conductors whereas the oxides of the fourth row elements exhibit very limited conductive phases. The most commonly used post-transition-metal oxides (ZnO, SnO_2 and In_2O_3) are thus serving as transparent conducting oxide (TCO) electrodes in opto-electronic devices [1,2]. However, the recent growing demands for high-performance and low-cost TCO has led to an extensive search for alternate TCO materials with higher transparency and conductivity [3–5].

A working hypothesis has been proposed for finding some technologically important transparent and electro-conductive spinel oxides [6]. According to this hypothesis, transparent conducting oxides like; $MgIn_2O_4$ [7], $CdGa_2O_4$ [8], $ZnGa_2O_4$ [9], Zn_2SnO_4 [10] and few more have been studied recently. Among these ternary oxides, $MgIn_2O_4$ thin films find potential application as a promising transparent as well as active electrode in photo-electrochemical solar cells [11]. It is an n-type wide-band gap semiconductor, which has a separate conducting path in the crystal lattice. It has the general

Table 1
Optimized spray deposition conditions for preparing spinel MgIn$_2$O$_4$ films

Spray parameters	Values/quantity
Solvent	100% ethanol
Substrate temperature	400–450 °C
Carrier gas flow rate	0.4 kg/cm^2
Substrate to nozzle distance	30 cm
Time of deposition	10 min
Precursor flow rate	5 ml/min

structure like the mineral spinel MgAl$_2$O$_4$ with the formula AB$_2$O$_4$. It falls under inverse spinel category, according to the lattice substitution of A and B cations in the tetrahedral and octahedral voids in the fcc-cp oxygen sub-lattice. Unit cell of MgIn$_2$O$_4$ contains eight formula units (Z=8) corresponding to the formula Mg$_8$In$_{16}$O$_{32}$. The coordination environments of Mg^{2+} and In^{3+} are entirely different from normal spinel because they are introduced into the inverse spinel structure.

An interesting phenomena observed in this spinel structure is that the number of cations occupying the 8a and 16d sites may vary. Half of the In^{3+} ions are placed in tetrahedral 8a sites. The other half of In^{3+} ions and all the Mg^{2+} ions are occupying the octahedral 16d sites due to which the occupancy of them observed is distorted. Intermediate phases also exist with the formula (A$_{1-x}$B$_x$)[A$_x$B$_{2-x}$]O$_4$ [12]. These films are found to exhibit higher values of electrical conductivity due to electrons generated from oxygen vacancies even without intentional doping [13] and/or from implanting Li$^+$ and H$^+$ ions into the crystal lattice [6].

Preparation of such thin films on quartz substrate is essentially important for estimating their reproducible and reliable structural, optical and electrical properties. Different techniques of deposition have been reported for preparing magnesium indate (MgIn$_2$O$_4$) by pulsed laser deposition [14], combustion synthesis [15] and magnetron sputtering [16–18]. Spray pyrolysis is a simple and elegant technique for large area preparation of TCO thin films. In the present paper, the preparation of MgIn$_2$O$_4$ spinel thin films by spray pyrolysis technique for various cationic ratios and their structural evaluation, variations in electrical and optical properties are reported.

2. Experimental details

The spray pyrolysis set-up and the detailed procedure adopted for the deposition of MgIn$_2$O$_4$ thin films have been described elsewhere [19]. Magnesium acetate and indium chloride were taken as the precursors for the preparation of MgIn$_2$O$_4$ film. The precursors were dissolved in ethanol to give a metal concentration of 0.1 mol/l. The mole ratio of precursors in solutions was Mg/In=0.35, 0.40, 0.45 and 0.50. The spray solution was always buffered by a small amount of hydrochloric acid to increase the solubility of the solution and sprayed on to quartz substrates heated at 450 °C. The required deposition parameters to obtain high quality films were optimized by controlling the associated process parameters and are listed in Table 1. The reproducibility was ascertained by measuring the experimental data on several samples prepared under nearly identical conditions. All the films prepared have a thickness of 0.32–0.46 μm as estimated by the Stylus profilometer (Mitutoyo).

The structural aspects were investigated by X-ray diffraction (XRD) (PANalytical-3040 X'pert Pro) using Ni filtered CuK$_\alpha$ radiation (λ=1.5408 Å) in θ–2θ scanning mode. Rutherford back scattering (RBS) spectra were recorded for the MgIn$_2$O$_4$ films prepared for different cationic ratios (Mg/In). In the present study, a tandem peletron accelerator was set-up to deliver ions of 3.05 MeV He$^+$ for the detection of back scattered yield. The chemical composition and binding states of the magnesium indium oxide films deposited at the optimized deposition conditions with Mg/In ratio 0.5 was characterized by X-ray photoelectron spectroscopy (XPS) over an area of about 1 mm×1 mm using a PHI 5600ci ESCA spectrometer with facilities for

excitation of photoelectrons using monochromated Al-K$_\alpha$ or Mg-K$_\alpha$ X-rays. For the present investigations, XPS spectra were recorded engaging Al-K$_\alpha$ (1486.6 eV) radiation from an X-ray source operated at 12 kW, 10 mA. The film was sputter-cleaned by Ar$^+$ etching (5 kV, 15 μA) prior to recording the XPS spectrum. Survey spectrum scan up to 1400 eV along with high resolution 23.5 eV scans were recorded for the Mg 1s, In 3d, O 1s, and C 1s peaks. Freeware tool "XPS Peak" was used for analyzing the XPS data which were calibrated against the C 1s peak at 284.5 eV. Using Tougaard's method [20], the background was subtracted from each peak before fitting. Gaussian–Lorentzian sum-functions software was used for peak-fitting. The high resolution spectra were recorded at a constant analyzer energy, which made the detector efficiency constant and the analyzer resolution as 0.6 eV full width at half-maximum (FWHM). For the monochromatic Al-K$_\alpha$ radiation, the resolution of the FWHM was set at ≥0.6 eV. Optical transmittance measurements were performed with a Hitachi-330 UV–Vis–NIR spectrophotometer in the wavelength range of λ=280–1500 nm. The sheet resistance and direct current (dc) conductivity (σ) were measured using the four-probe method at different temperatures (30–150 °C) using Keithley 2000 multimeter and Oriel 70310 multifunction meter. The effective carrier concentration and mobility were calculated using Hall effect measurements.

3. Results and discussion

3.1. Structural identification of the spinel phase

MgIn$_2$O$_4$ films prepared for different cationic ratios were characterized using XRD in order to get information about the crystallographic evolution of spinel structure and orientation of crystallites. The XRD patterns recorded on MgIn$_2$O$_4$ films prepared for different
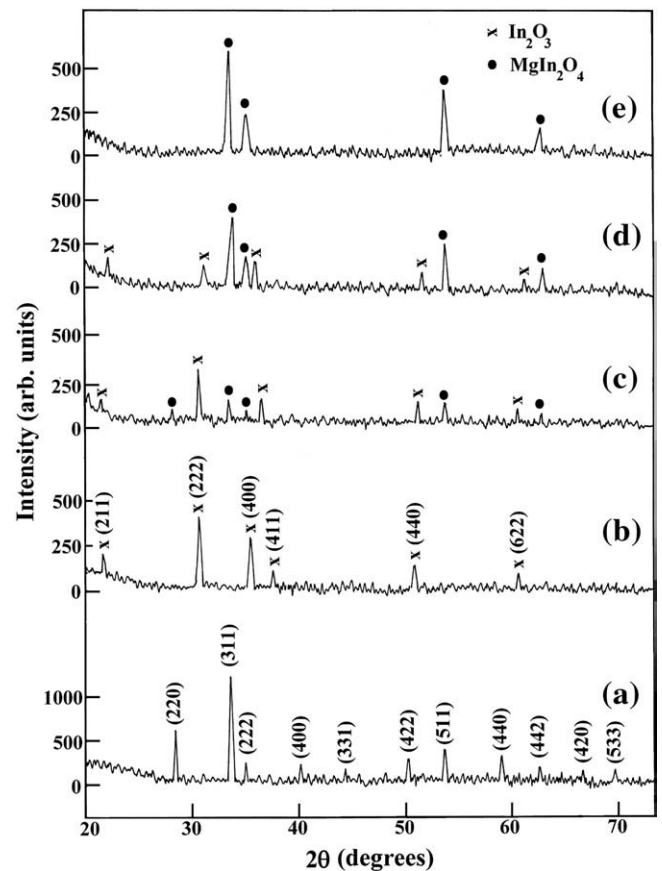

Fig. 1. XRD patterns of MgIn$_2$O$_4$ films prepared with different Mg/In ratios (a) MgIn$_2$O$_4$ powder sample (b) Mg/In=0.35 (c) Mg/In=0.40 (d) Mg/In=0.45 (e) Mg/In=0.50.

Table 2
XRD data of $MgIn_2O_4$ films prepared with different cationic ratios

Cationic ratio (Mg/In)	Diffraction angle (2θ) degree		Miller indices (hkl)		Relative Intensity (%)		Observed unit cell dimension a (Å)		Standard unit cell dimension a (Å)	
	In_2O_3 phase	$MgIn_2O_4$ phase	In_2O_3 phase	$MgIn_2O_4$ phase	In_2O_3 phase	$MgIn_2O_4$ phase	In_2O_3	$MgIn_2O_4$	In_2O_3	$MgIn_2O_4$
0.35	21.58	–	(211)	–	31.67	–	10.108(4)	–	10.118	8.864
	30.67		(222)		100					
	35.50		(400)		76.72					
	37.70		(411)		26.21					
	51.08		(440)		24.19					
	60.68		(622)		20.61					
0.40	21.57	27.84	(211)	(220)	8.62	6.78	10.11(1)	9.03(2)	10.118	8.864
	30.84	32.46	(222)	(311)	75.61	24.71				
	35.49	34.10	(400)	(222)	28.62	8.21				
	51.03	52.56	(440)	(511)	20.86	22.64				
	60.59	61.83	(622)	(442)	12.42	6.62				
0.45	22.09	32.58	(211)	(311)	8.21	94.6	10.01(1)	9.06(1)	10.118	8.864
	31.08	34.19	(222)	(222)	34.18	36.26				
	35.98	52.61	(400)	(511)	18.41	56.72				
	51.56	61.93	(440)	(442)	16.87	24.76				
	61.21		(622)		9.26					
0.5	–	33.42	–	(311)	–	100	–	8.887(2)	10.118	8.864
		34.91		(222)		41.60				
		53.51		(511)		62.81				
		62.69		(442)		20.69				

Mg/In ratios are shown in Fig. 1. Diffraction data were collected by step scanning over the angular range of $20° \le 2\theta \le 80°$ in increments of $0.04°$ in 2θ. The diffraction pattern indicates that the films are polycrystalline and strongly dependent on the cationic proportion in the spray solution. The films prepared for the cationic ratio=0.35 exhibited peaks at $2\theta = 21.58°$, 30.67°, 35.50°, 37.70°, 51.08° and 60.68° respectively for (211), (222), (400), (411), (440) and (622) planes that corresponds to indium oxide phase only. The relative intensity and the unit cell dimensions observed are listed in Table 2.

The lattice parameter a of the single-phase In_2O_3 films evaluated after refinement of all the observed peaks is 10.108 Å, which is slightly less than the bulk value (10.118 Å). Since the octahedral site preference energy of In^{3+} is small of the order of -40 kcal g^{-1} atomic weight [21], it dominates in forming In_2O_3 than $MgIn_2O_4$. The films prepared with $\left(\frac{Mg}{In}\right) = 0.4$ contained both In_2O_3 and $MgIn_2O_4$ phases. On comparing the relative intensity of the peaks, the secondary phase In_2O_3 is dominating than the required primary phase $MgIn_2O_4$. The peak positions of the $MgIn_2O_4$ phase were compared with the standard
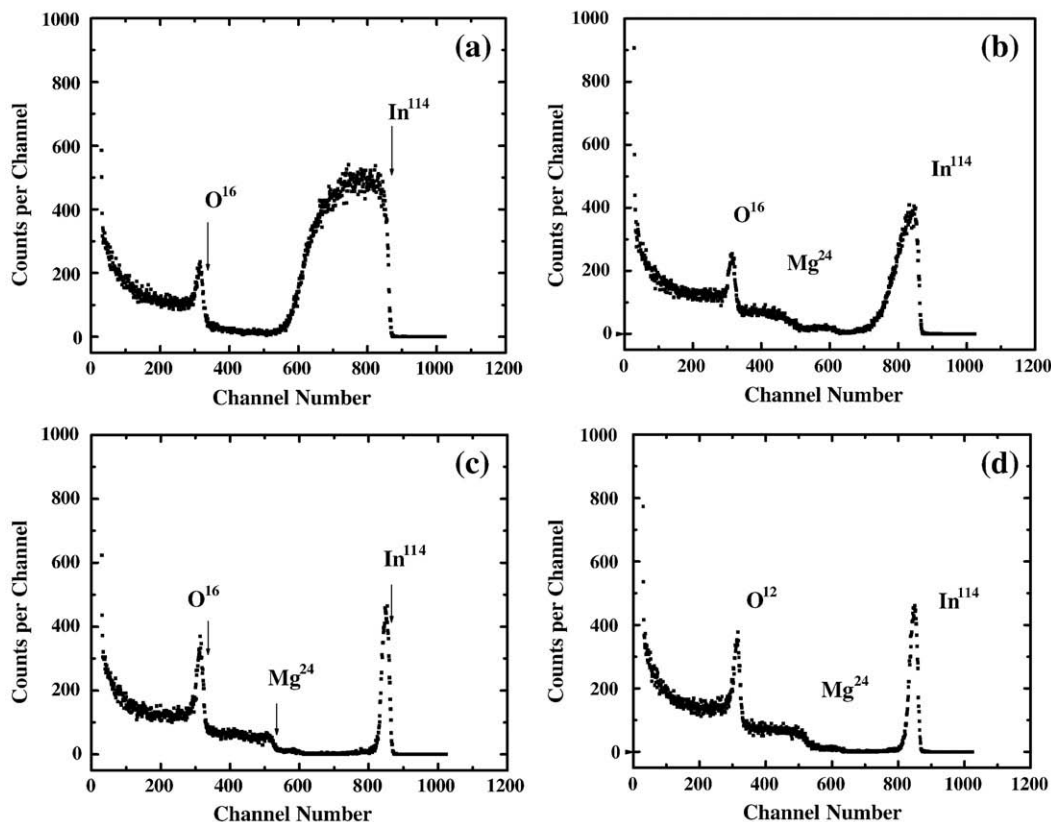
Fig. 2. RBS spectra of $MgIn_2O_4$ films deposited for different cationic ratio (Mg/In): (a) 0.35 (b) 0.40 (c) 0.45 (d) 0.50. Thicknesses of the films are 451 nm, 421 nm, 409 nm and 423 nm, respectively.

peaks of the MgIn$_2$O$_4$ powder (JCPDS card No.73-2414) [22]. The peak positions are slightly shifted to the low angle side of the standard peaks indicating the increase in their interplanar distance d resulting higher unit cell parameter a =9.03 Å against 8.864 Å, the bulk value. However, unit cell dimension of In$_2$O$_3$ phase is decreased (10.11 Å). For higher indium rich compositions, the indium oxide phase is dominant and was reported earlier by Tanji et al. [23] for the MgIn$_2$O$_4$ films prepared from calcination of In$_2$O$_3$ and MgCO$_3$ powder. Similar secondary phase formation was reported for many of the spinel compounds: CdIn$_2$O$_4$ [24], MgGa$_2$O$_4$ [25] and MgAl$_2$O$_4$ [26].

Further rise in $\left(\frac{Mg}{In}\right) = 0.45$ increases the intensity of the MgIn$_2$O$_4$ peak exhibiting the dominance of magnesium indate phase than the In$_2$O$_3$ phase formation comparatively. The peak intensity of the In$_2$O$_3$ phase is very low (Fig. 2(d)). The positions of the MgIn$_2$O$_4$ slightly shifted towards the standard values thereby reducing the unit cell parameter. At $\left(\frac{Mg}{In}\right) = 0.5$, the indium oxide phase disappeared completely, bearing only single spinel magnesium indium oxide phase. The peaks at 33.42°, 34.91°, 53.51° and 62.69° are respectively arising from the diffraction planes (311), (222), (511) and (442) of MgIn$_2$O$_4$. The lattice parameter of the single-phase MgIn$_2$O$_4$ film evaluated after cell refinement is 8.887 Å against the bulk value 8.864 Å. These observations confirmed that the optimized cationic ratio for the single-phase MgIn$_2$O$_4$ evolution is exactly $\left(\frac{Mg}{In}\right) = 0.5$.

The structural evolution of MgIn$_2$O$_4$ was further confirmed with the aid of the Rutherford backscattering spectrometry. In the present study, Rutherford backscattering spectra were recorded for the MgIn$_2$O$_4$ films prepared for different cationic ratios (Mg/In) at the substrate temperature of 450 °C. A 3.05 MeV He$^+$ ion beam line had been used in all the cases and the beam was normal to the sample. The scattered particles were analyzed with a solid-state detector located about 10 cm from the target and with a solid angle between 3 and 4 msr. A multi-channel analyzer was used to record the back scattered ions with a channel width of 3 keV. Fig. 2 shows a typical RBS spectrum of MgIn$_2$O$_4$ films deposited on quartz substrate at 450 °C for different cationic ratios.

Thin films prepared with cationic ratio (Mg/In) 0.35 in precursor solution forms only indium oxide instead of magnesium indium oxide. This result has been confirmed again through the RBS studies (Fig. 2a). The peak at the respective position corresponding to the elements indium and oxygen confirms the formation of In$_2$O$_3$ films with out any mixed phases like MgO and/or MgIn$_2$O$_4$. However, the films deposited with cationic ratios 0.4 and 0.45 (Fig. 2b, c) have certain minimum magnesium ion yield indicating the formation of MgIn$_2$O$_4$ along with In$_2$O$_3$. The mixed phase formation is already confirmed from the XRD studies. As the Mg content in the precursor increases further so that Mg/In=0.5, the magnesium yield also increases correspondingly as seen in Fig. 2d. It is observed that the Mg yield is zero for the films prepared with cationic ratio 0.35. For the other cationic ratios (>3.5), the indium yield is dominating with certain low yield for the magnesium component. This may be the reason to have mixed phases of In$_2$O$_3$ and MgIn$_2$O$_4$ for these cationic proportions. For the cationic ratio of 0.5, the magnesium yield is increased to have the stoichiometric spinel film that was confirmed from the elemental composition analysis to be discussed in the next section. The gradual increases in oxygen yield is also an indication for the formation of good quality and nearly stoichiometric MgIn$_2$O$_4$ films.

3.2. Elemental composition analysis

The chemical composition and binding states of the magnesium indium oxide film deposited at the optimized deposition conditions with Mg/In ratio 0.5 was characterized by XPS using Al-K$_\alpha$ radiations at 1486.6 eV. In Fig. 3, the binding energy survey spectrum of the scattered electron density per unit energy interval is displayed for the magnesium indium oxide film deposited at the substrate temperature of 450 °C. The binding energies were corrected to compensate for any
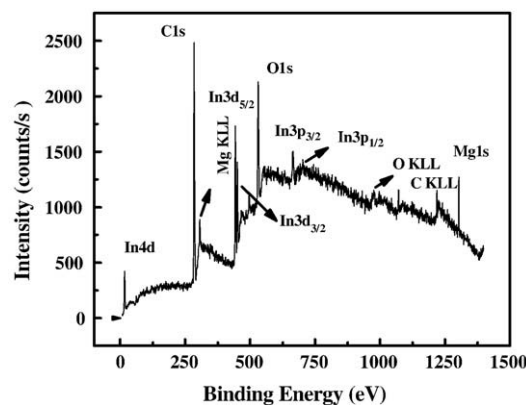

Fig. 3. XPS survey spectrum of magnesium indium oxide film.

charge induced shifts by setting the C 1s signal to 284.5 eV. Obtained values are in good agreement with the reported values [27,28]. In addition, the core level spectra of Mg 1s, In 3d$_{3/2}$, In 3d$_{5/2}$, In 4d and O 1s are shown in Fig. 4. Assuming the intensity distribution to be Gaussian, peak-fitting technique was employed for accurate area measurements to calculate the stoichiometry of the deposited MgIn$_2$O$_4$ film. For analyzing XPS data, the freeware tool 'XPS peak' is used and the data are calibrated against the C 1s peak at 284.5 eV. Also, for peak-fitting, the Gaussian–Lorentzian sum function is used. The ratio between two elements was calculated using the formula: $\frac{n_1}{n_2} = \frac{I_1 S_2}{I_2 S_1}$, where, n is the number of atoms per cm^3, I is the intensity of the XPS peak and S is the atomic sensitivity factor. The atomic sensitivity factor for each of the XPS lines are taken from the reported results previously [29,30].

The peak corresponding to Mg 1s is located at BE 1303.39 eV (Fig. 4a). Fig. 4b shows the XPS spectrum of the peaks of In 3d doublet (In 3d$_{5/2}$ and In 3d$_{3/2}$). The binding energy of In 3d$_{5/2}$ is at 443.32 eV, which corresponds to the indium bonding with oxygen [31]. Similar to indium 3d doublet, indium 4d peak position is illustrated in Fig. 4c. Fig. 4d shows the results from a fitting of an XPS of O 1s in MgIn$_2$O$_4$ thin film. The experimental contour of oxygen spectrum fits three peaks centering at 529.05 eV, 531.4 eV and 532.35 eV. Jupile et al. [32] investigated O 1s core levels of alkaline metal oxides by comparing binding energy differences between the valence band and core level. The O 1s binding energy reported are located at 527–531 and 530–532 eV for alkaline metal oxide (O^{2-}) and peroxide (O$_2^{2-}$) respectively. The difference in binding energy or chemical shift is due to an appreciable change of the electronic charges surrounding O atoms between the O^{2-} and O$_2^{2-}$ configurations [33]. On the basis of these reported results, the peaks centered at 529.05 eV and 531.4 eV are assigned to the metal oxide (Mg^{2+}–O^{2-}) binding and metal peroxide (Mg–O$_2$) binding respectively. The other state is assigned to the bond formation of indium with oxygen atoms (532.35 eV, In–O–In) [34]. However, the peroxide bond peak located at 531.4 eV can also be assigned to the contamination of the surface with carbon compounds (C–OH) [35,36]. As revealed in Fig. 4e, deconvolution of carbon C 1s spectrum has two peaks; the first one is located at 284.61 eV that corresponds to carbon C–C/C–H, the second corresponds to the liaisons with oxygen atom at 285.28 eV [36].

From these observations, the ratio between magnesium and oxygen is of the order of 0.26. In addition, the XPS spectrum shows that, although film deposition is carried out in air without additional oxygen purging, there is no evidence of oxygen deficiency in the resulting peaks. These results indicate that oxygen is not only captured during the film deposition from air but also from the precursor. From the Mg 1s and In 3d$_{5/2}$ narrow scan XPS peaks, the Mg/In atomic ratio is estimated to be 0.46 and this is nearer to the expected values of 0.5. This result also confirms the perfect stoichiometry of the prepared single-phase MgIn$_2$O$_4$ film.

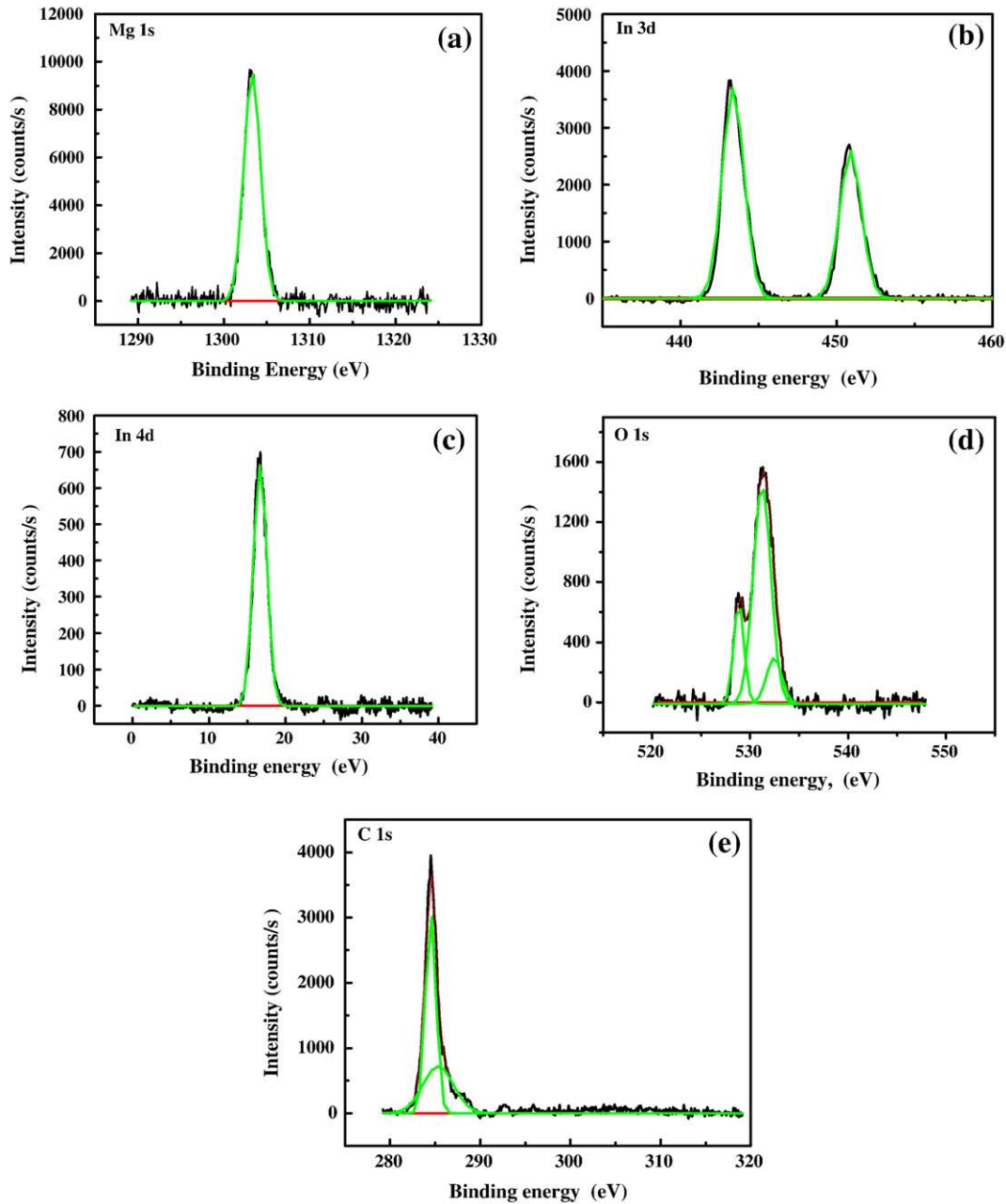**Fig. 4.** XPS spectra of $MgIn_2O_4$ film deposited at 450 °C with Mg/In=0.5: (a) Mg 1s spectrum (b) In 3d spectrum (c) O In 4d spectrum (d) O 1s spectrum and (e) C 1s spectrum.

3.3. Optical characterization

Fig. 5 shows the transmittance spectra of $MgIn_2O_4$ films deposited at 450 °C for various Mg/In ratios in the precursor. It is observed that, the % transmittance of the indium rich films are more compared to that of the $MgIn_2O_4$ film prepared under the optimized deposition conditions with cationic ratio Mg/In=0.5. For the indium rich films, the In_2O_3 phase formation may be the reason for more transmittance. A maximum transmittance of 86.2% is observed at 600 nm for the films prepared with Mg/In=0.35. For this cationic ratio, prepared films are In_2O_3 instead of $MgIn_2O_4$, which is already confirmed from the XRD and RBS studies. Further increase in Mg species induces the formation of $MgIn_2O_4$ phases and thus the transmittance is gradually decreased. Alternately, changes in the optical transmittance in turn induce changes in optical band gap energy and these changes have been observed for different Mg/In ratios. Inset of Fig. 5 shows the variation of band gap energy with addition of magnesium. The
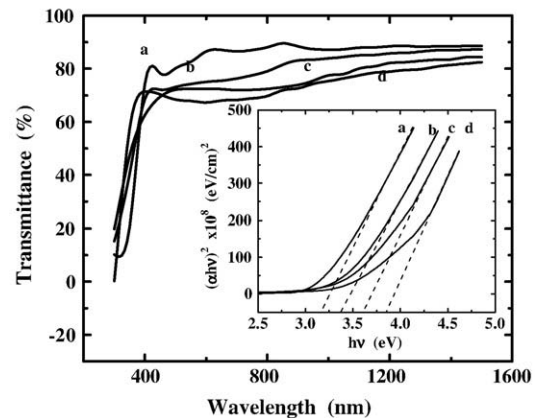

Fig. 5. Transmittance spectra of $MgIn_2O_4$ films prepared for different cationic ratios. Inset shows the optical band gap variations.

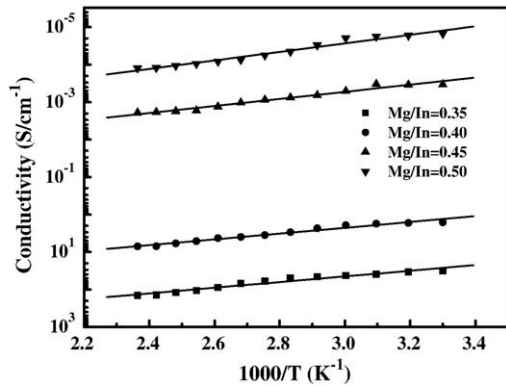**Fig. 6.** Electrical conductivity variations with temperature in $MgIn_2O_4$ films deposited for different cationic ratios (Mg/In).

Table 3
Variation of activation energy (E_a) for different cationic ratios (Mg/In) in $MgIn_2O_4$ films

Cationic ratio (Mg/In)	Activation energy (E_a) eV
0.35	0.35
0.40	0.353
0.45	0.43
0.50	0.52

absorption edge is shifted to short wavelengths as the Mg content is increased. This indicates that the band gap of the films widens as the Mg content is increased. The increase in optical band gap energy with the addition of Mg is already reported for the $Mg_xZn_{1-x}O$ alloy thin films [37–40].

It is evident that the % transmittance decreases as 86.2, 74.8, 72.4, and 66.9%, where as the optical band gap energy increases as 3.18, 3.38, 3.62 and 3.86 eV with the cationic ratio (Mg/In) of 0.35, 0.40, 0.45 and 0.50 respectively. The increase of optical band gap with Mg content is once again verified in the present study, which in turn also confirms the single-phase formation of spinel $MgIn_2O_4$ films.

3.4. Electrical characterization

The dependence of electrical conductivity of spray deposited $MgIn_2O_4$ films prepared from various cationic ratio precursors is shown in Fig. 6. The dc electrical conductivity increases from 10^{-5} to 10^2 S cm^{-1} with decreasing cationic ratio from 0.50 to 0.35 respectively. The maximum dc conductivity of 34.07 S cm^{-1} is attained in the films deposited for Mg/In=0.35. This value is about 6 orders higher than that of $MgIn_2O_4$ films deposited with Mg/In=0.5, whose value is 1.44×10^{-5} S cm^{-1}. This vast increase of electrical conductivity for a small fractional increase in Mg/In is attributed to the formation of highly conducting In_2O_3 phase in the film. It is evident from XRD and RBS analysis that the films deposited with Mg/In=0.35 (indium rich) have exhibited only the In_2O_3 phase without any additional phases like MgO and/or $MgIn_2O_4$. The obtained electrical conductivity is in agreement with the reported result of Siefert [41] and Mihaela Girtan [42] for the sprayed In_2O_3 films with thicknesses of same order (0.4 μm).

As the concentration of Mg species increases, the conductivity of the $MgIn_2O_4$ decreases rapidly and attain the value 1.44×10^{-5} S cm^{-1} for the films deposited with Mg/In=0.5. These films exhibited only the $MgIn_2O_4$ phase with better crystallinity. Usually in spinel semiconductor films, current carriers are generated from oxygen vacancies [13]. Decreased electrical conductivity of the prepared $MgIn_2O_4$ films are therefore attributed to the stoichiometric films with less oxygen ion vacancies. Similar observations ($\sigma \approx 10^{-5}$–10^{-7} S cm^{-1}) are reported for the magnesium indium oxide films prepared using the RF (radio frequency) sputtering technique [18,43,44]. In addition, lower conductivity reveals less concentration of the conduction electrons that in turn demonstrate the non-degenerate semiconducting nature of electrical conduction in stoichiometric $MgIn_2O_4$ films.

In addition, it is evidenced from Fig. 6 that the electrical conductivity decreases as the Mg content is increased in the precursor. This may be due to the increase of band gap energy with the increase of magnesium content. The band gap of $MgIn_2O_4$, having the basic cubic structure, widens from 3.18 to 3.86 eV as Mg/In varies from 0.35

to 0.5. Minemoto et al. [39] also reported similar type of electrical conduction variations of magnesium zinc oxide thin films as a function of Mg content. Further, it is observed that the electrical resistivity of the films with different Mg/In ratios is decreasing when the temperature is increased from 30 to 150 °C which confirm the semiconducting nature of all the films. For the regions in which the electrical resistivity decreases with the increase of the temperature, the well-known dependence of semiconductor electrical conductivity on temperature is considered: $\sigma = \sigma_o \exp(-E_a/2kT)$ where, E_a denotes the thermal activation energy of electrical conduction, σ_o represents a parameter depending on the semiconductor nature and k is the Boltzmann constant. The activation energy values calculated using the regression curves fitted for the data points in the graph (Fig. 6) drawn between conductivity σ and $\left(\frac{1000}{T}\right)$ and are listed in Table 3. Comparatively, spray deposited films with cationic ratio Mg/In=0.5 have higher activation energy of 0.52 eV than the films with Mg/In=0.35 whose value is 0.35 eV. Indium rich films are therefore more conductive than that of magnesium rich films. Therefore, the stoichiometric $MgIn_2O_4$ films require more thermal energy to transfer an electron from impurity level to the conduction band.

In the present study, carrier concentration and mobility values of the $MgIn_2O_4$ films were obtained at room temperature under thermal equilibrium conditions. Hall mobility measurements indicate n-type conduction in all the prepared films. The variation of Hall mobility and carrier concentration of $MgIn_2O_4$ films prepared with different Mg/In ratio is shown in Fig. 7. The carrier concentration of $MgIn_2O_4$ films with excess indium decreased with increasing Mg/In ratio. Also in inverse spinel structure of $MgIn_2O_4$, as the Mg/In ratio increases, more octahedral sites will be occupied with Mg either in neutral or ionized state. These octahedral sites act as scattering centers for the conduction electron and reduce the electrical conductivity. For the $MgIn_2O_4$ films with Mg/In=0.5, the mobility is of the order of 10^{-3} cm^2 V^{-1} s^{-1}, which again reduces the conductivity to a minimum of 1.5×10^{-5} S cm^{-1}. It is obvious that stoichiometric films with less oxygen vacancies exhibit lower electron mobility indicating a hopping type of conduction mechanism. This is corroborated by the observed electron mobility variations. One such result is reported for the sintered and stoichiometric $MgIn_2O_4$ film [21]. Increase of electrical conductivity in $MgIn_2O_4$
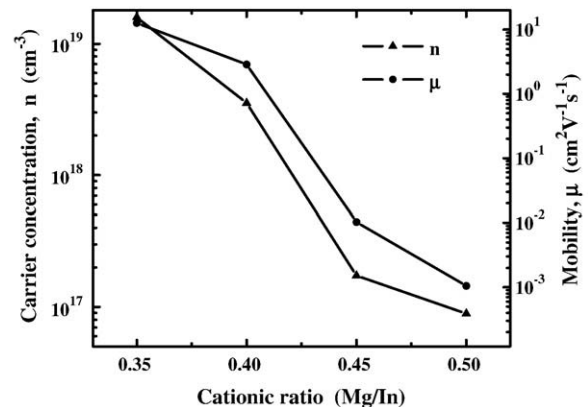

Fig. 7. Variation of carrier concentration and Hall mobility of $MgIn_2O_4$ films with different Mg/In ratios.

films can be achieved by increasing the carrier concentrations or mobility using ion implantation or preparing non-stoichiometry films with oxygen ion vacancies, which will be under exploration.

4. Conclusion

Highly transparent and semiconducting films of magnesium indium oxide have been prepared by chemical spray pyrolysis technique. The structural, optical and electrical properties of the films are found to be very sensitive to the cationic ratio in the precursor. The films deposited at 450 °C with the cationic ratio in precursor 0.5 are identified as single-phase $MgIn_2O_4$ with an inverted spinel structure. Mixed phases of In_2O_3 and $MgIn_2O_4$ are observed in the films prepared with cationic ratios 0.4 and 0.45. Single-phase In_2O_3 film is obtained for the cationic ratio 0.35. These results are further confirmed from the results of the RBS, optical and electrical characterizations. The optical transmittance variations from 86–66% and optical band gap variations in the range 3.18–3.86 eV are observed as the cationic ratio is varied from 0.35 to 0.5. Increase in optical band gap and decrease in optical transmittance in the $MgIn_2O_4$ films are due to the incorporation Mg species that leads to well stoichiometric and single-phase films. The electrical conductivity also has a strong dependence to the cationic ratio. In spinel structure, more number of octahedral and tetrahedral vacancies are available and therefore its conductivity can be increased by incorporation of dopant by ion implantations or by creating oxygen ion vacancies.

References

[1] I. Hamberg, C.G. Granqvist, J. Appl. Phys. 60 (1986) R123.
[2] T. Minami, H. Sato, H. Nanto, S. Takata, Jpn. J. Appl. Phys. 24 (1985) L781.
[3] Y. Dou, G. Egdell, Phys. Rev. B53 (1996) 15405.
[4] K. Budzynska, E. Leja, S. Skrztpek, Sol. Energy Mater. 12 (1985) 57.
[5] D.R. Kammler, T.O. Mason, D.L. Young, T.J. Coutts, D. Ko, K.R. Poeppelmerer, D.L. Williamson, J. Appl. Phys. 90 (2001) 5979.
[6] H. Kawazoe, N. Ueda, H. Un'no, T. Omata, H. Hosono, H. Tanoue, J. Appl. Phys. 76 (1994) 7935.
[7] N. Ueda, T. Omata, N. Hikuma, K. Udea, H. Mizoguchi, T. Hashimoto, H. Kawazoe, App. Phys. Lett. 61 (1992) 1954.
[8] T. Omata, N. Ueda, N. Hikuma, K. Udea, H. Mizoguchi, T. Hashimoto, H. Kawazoe, App. Phys. Lett. 62 (1993) 499.
[9] T. Omata, N. Ueda, K. Ueda, H. Hawazoe, App. Phys., Lett. 64 (1994) 1077.
[10] H. Enoki, T. Nakayama, J. Echigoya, Phys. Status Solidi (a) 129 (1992) 181.
[11] P.M. Sirimanne, N. Sonoyama, T. Sakata, J. Sol. State Chem. 154 (2000) 476.
[12] S.-H. Wei, S.B. Zhang, Phys. Rev. B63 (2001) 45112.
[13] H. Un'no, N. Hikuma, T. Omata, N. Ueda, T. Hashimoto, Kawazoe, Jpn. J. Appl. Phys. 32 (1993) 1260.
[14] A. Kudo, H. Yanagi, H. Hosono, H. Kawazoe, Mater. Sci. Engin. B54 (1998) 51.
[15] N. Ueda, T. Omata, N. Hikuma, K. Ueda, H. Mizoguchi, T. Hashimoto, H. Kawazoe, Appl. Phys. Lett. 61 (1992) 1954.
[16] T. Minami, S. Takata, T. Kakumu, H. Sonohara, Thin Solid Films 270 (1995) 22.
[17] H. Un'no, N. Hikuma, T. Omata, N. Ueda, T. Hashimoto, H. Kawazoe, Jpn. J. Appl. Phys. 32 (1993) L1260.
[18] H. Hosono, H. Un, 'no, N. Ueda, H. Kawazoe, N. Matsunami, H. Tanoue, Nuclear Instr. Methods Phys. Res. B106 (1995) 517.
[19] J.J. Prince, S. Ramamurthy, B. Subramanian, C. Sanjeeviraja, M. Jayachandran, J. Cryst. Growth 240 (2002) 142.
[20] S. Tougaard, J. Electron Spec. Relat. Phenom. 52 (1990) 243.
[21] A. Paul, S. Basu, Trans. Br. Ceram. Soc. 73 (1974) 167.
[22] Powder Diffraction File, Joint-Committee on Powder Diffraction Standards, Philadelphia, PA (1974–present).
[23] H. Tanji, N. Kurihara, M. Yoshida, J. Mater. Sci. Lett. 13 (1994) 1673.
[24] P. Mohan Babu, G. Venkata Rao, S. Uthanna, Mater. Chem. Phys. 78 (2002) 208.
[25] T. Moriga, T. Sakamoto, Y. Sato, A.H. Khalid @ Haris, R. Suenari, I. Nakabayashi, J. Sol. State Chem. 142 (1999) 206.
[26] A. Ghosh, R. Sarkar, B. Mukherjee, S.K. Das, J. Eur. Ceram. Soc. 24 (2004) 2079.
[27] T.-Y. Chou, Y.C.S.-F. Huang, C.-S. Liu, Inorg. Chem. 42 (2003) 6041.
[28] T. Satoh, H. Fujikawa, Y. Taga, Appl. Phys. Lett. 87 (2005) 143503.
[29] J.F. Moulder, Handbook of X-ray Photoelectron Spectroscopy, Perkin-Elmer Corporation, Physical Electronics Division, 1992.
[30] C.D. Wagner, L.E. Davis, M.V. Teller, J.A. Taylor, R.H. Raymond, L.H. Gale, Surf. Interface Anal. 3 (1981) 211.
[31] M.D. Stoev, J. Tousek, Thin Solid Films 299 (1997) 67.
[32] J. Jupile, P. Dolle, M. Besançon, Surf. Sci. 260 (1992) 271.
[33] J.C. Fuggle, LM. Watson, D.J. Fabian, S. Affrossman, Surf. Sci. 49 (1975) 61.
[34] J.F. Moulder, W.F. Stickle, P.E. Sobol, K.D. Bomben, in: J. Chastain, R.C. King Jr. (Eds.), Handbook of X-ray Photoelectron Spectroscopy, Physical Electronics, Eden Prairie, MN, 1995.
[35] D.T. Clark, I. Scanlan, J. Muller, Theor. Chim. Acta. 35 (1974) 341.
[36] D.T. Clark, A. Dilks, J. Polym. Sci. 17 (1979) 957.
[37] Y. Zhang, G. Du, D. Liu, H. Zhu, Y. Cui, X. Dong, S. Yang, J. Cryst. Growth 268 (2004) 140.
[38] T. Minemoto, T. Negami, S. Nishiwaki, H. Takakura, Y. Hamakawa, Thin Solid Films 372 (2000) 173.
[39] T. Minemoto, N. Ichiba, S. Sasa, M. Inoue, Thin Solid Films, 486 (2005) 174.
[40] A. Ohtomo, M. Kawasaki, T. Koida, K. Masubuchi, H. Koinuma, Y. Sakurai, Y. Yoshida, T. Yasuda, Y. Segawa, Appl. Phys. Lett. 19 (1998) 2466.
[41] W. Siefert, Thin Solid Films 121 (1984) 275.
[42] M. Girtan, Surf. Coat. Technol. 184 (2004) 219.
[43] H. Kawazoe, N. Ueda, H. Un'no, T. Omata, H. Hosono, H. Tanoue, J. Appl. Phys. 76 (1994) 7935.
[44] H. Hosono, N. Ueda, H. Kawazoe, N. Matsunami, J. Non-Cryst. Sol. 182 (1995) 109.